HHS Public Access

Author manuscript

J Magn Reson Imaging. Author manuscript; available in PMC 2021 January 01.

Published in final edited form as:

J Magn Reson Imaging. 2020 January ; 51(1): 296–310. doi:10.1002/jmri.26792.

Distortion-Free Imaging: A Double Encoding Method (DIADEM) combined with Multi-Band Imaging for Rapid Distortion-Free High-Resolution Diffusion Imaging on a Compact 3T with High-Performance Gradients

Myung-Ho In, PhD[1], **Ek Tsoon Tan, PhD**[2], **Joshua D Trzasko, PhD**[1], **Yunhong Shu, PhD**[1], **Daehun Kang, PhD**[1], **Uten Yarach, PhD**[1], **Shengzhen Tao, PhD**[1], **Erin M Gray, RT**[1], **John Huston III, MD**[1], **Matt A Bernstein, PhD**[1]

[1]Department of Radiology, Mayo Clinic, Rochester, MN, United States

[2]GE Global Research, Niskayuna, NY, United States

Abstract

Background: Distortion-free, high-resolution diffusion imaging using DIADEM (Distortion-free Imaging: A Double Encoding Method) proposed recently has great potential for clinical applications. However, it can suffer from prolonged scan times and its reliability for quantitative diffusion imaging has not been evaluated.

Purpose: To investigate clinical feasibility of DIADEM-based high-resolution diffusion imaging on a novel compact 3T (C3T) by evaluating the reliability of quantitative diffusion measurements and utilizing both the high-performance gradients (80 mT/m, 700 T/m/s) and the sequence optimization with the navigator acquisition window reduction and simultaneous multislice (multi-band) imaging.

Study Type: Prospective feasibility study.

Phantom/Subjects: Diffusion quality control phantom scans to evaluate the reliability of quantitative diffusion measurements; Thirty-six normal control scans for B0-field mapping; Six healthy and two patient subject scans with a brain tumor for comparisons of diffusion and anatomical imaging.

Field Strength/Sequence: 3T; the standard single-shot echo-planar-imaging (EPI), multi-shot DIADEM diffusion, and anatomical (2D-FSE, 2D-FLAIR, and 3D-MPRAGE) imaging.

Assessment: The scan time reduction, the reliability of quantitative diffusion measurements, and the clinical efficacy for high-resolution diffusion imaging in healthy control and brain tumor volunteers.

Statistical Tests: Bland-Altman analysis

Corresponding Author Information: Myung-Ho In, Ph.D., in.myungho@mayo.edu, Address: 200 First Street SW, Rochester, MN 55905, USA.

Results: The scan time for high in-plane (0.86 mm^2) resolution, distortion-free, and whole brain diffusion imaging were reduced from 10 to 5 minutes with the sequence optimizations. All of mean ADC values in phantom were within the 95% confidence interval in the Bland-Altman plot. The proposed acquisition with a total off-resonance coverage of 597.2 Hz wider than the expected bandwidth of 500 Hz in human brain could yield a distortion-free image without fold-over artifacts. Compared to EPI, therefore, this approach allowed direct image matching with the anatomical images and enabled improved delineation of the tumor boundaries.

Data Conclusion: The proposed high-resolution diffusion imaging approach is clinically feasible on the C3T due to a combination of hardware and sequence improvements.

Keywords

diffusion imaging; DIADEM; multi-shot EPI; distortion-free; geometric distortion; compact 3T

INTRODUCTION

Diffusion weighted imaging (DWI)[1] enables the diffusion of water molecules in tissue to be observed. The signal varies with tissue geometrical restrictions, and has been recognized as a valuable clinical tool, including for the evaluation of brain tumors.[2] Although single-shot, echo-planar imaging (EPI) is currently the most commonly-used foundation for clinical diffusion imaging, EPI is highly sensitive to magnetic field inhomogeneities as well as diffusion-pulse induced eddy-currents. When these non-idealities are not properly accounted for during image reconstruction, EPI based diffusion images can exhibit substantial geometric distortion and other image degradation, such as T2/T2* blurring. To minimize such artifacts, EPI readout trains are typically kept relatively short (e.g., 128), which limits their achievable spatial resolution. Because of these drawbacks, considerable interest has developed to simultaneously improve the spatial resolution and the image quality of DWI.

As an alternative to EPI, a novel, multi-shot approach,[3] referred herein as “distortion-free imaging: a double encoding method” (DIADEM), was recently proposed. In order to obtain high-resolution and distortion-free diffusion imaging, this approach adapted a double, spin-warp (SW) and EPI, phase-encoding (PE) strategy inspired by a point spread function (PSF) mapping technique.[4] This multi-shot approach fills in the additional SW-PE *k*-space dimension (k_s), providing additional signal averaging that benefits high-resolution imaging. In addition, the final image is reconstructed in the SW-PE (or distortion-free, *s*) rather than in the EPI-PE (or distorted, *y*) coordinate. This approach is – with minimal additional processing requirements over conventional EPI reconstruction – able to produce high-resolution diffusion-weighted (DW) images, essentially free from T2* blurring as well as susceptibility- and eddy-current-induced geometric distortion. This can offer an improvement over some other multi-shot approaches[5–7] that reconstruct images in the distorted EPI-PE coordinates. While the previous PSF mapping approaches[4,8–10] were applied as a calibration approach for EPI distortion correction, this DIADEM approach was proposed as an imaging approach.

Although distortion-free high-resolution imaging has great potential for clinical use, it can suffer from long scan times because additional EPI readouts are required in the SW-PE

dimension. Previously, a sub-sampling approach was introduced to accelerate the DIADEM acquisition with a reduced field of view (rFOV) in the SW-PE dimension, in conjunction with parallel imaging in the EPI-PE dimension.[3] Since the maximum FOV reduction is limited by the extent of distortion in the EPI-PE dimension,[9,10] further FOV reduction was achieved by minimizing the distortion using parallel imaging in the EPI-PE dimension.[3] Nevertheless, the scan time is still not practical for clinical use. Furthermore, the quantitative reliability of this approach for diffusion measurements had yet to be evaluated.

An alternative approach to minimizing distortion in conventional EPI is to utilize a higher-performance gradient system; specifically, one that has high slew-rate to reduce EPI echo spacing. While there are limitations to increasing the slew-rate due to peripheral nerve stimulation (PNS) thresholds on standard whole-body MRI systems, a compact, 42-cm inner diameter gradient coil has been demonstrated to provide significantly increased PNS thresholds.[11] The reduced inductance and resistance of the compact head-gradient system also relaxed the maximum voltage requirement of the gradient drivers, allowing higher gradient amplitudes (80 mT/m) and slew rates (700 T/m/s) to be achieved with only a standard 1 MVA per axis gradient driver system.[12] This system can provide considerably reduced image distortion and increased spatial resolution for single-shot EPI.[13] In addition, the compact 3T system provided similar level of acoustic noise as whole-body MRI systems, and passed standard image quality controls tests, such as those described by the American College of Radiology (ACR).[14,15]

The purpose of this work is to utilize the high slew-rate of the compact 3T and optimize the sequence in order to reduce the scan time of DIADEM, while achieving reliable image quality within clinically-acceptable scan times for diffusion imaging with whole-brain coverage and sub-millimeter in-plane resolution.

MATERIALS AND METHODS

DIADEM acquisition accelerated with high-performance gradients

DIADEM acquisition can be accelerated by reduced field of view (rFOV) imaging, which reduces the number of PE steps in the SW-PE dimension.[10] However, if there are too few PE steps, wraparound artifacts can occur. To obtain a distortion-free image without wraparound artifacts, the maximum allowable rFOV factor can be limited in the following manner:[9,10]

$$rFOV_{max} = N_s/\Delta(s), \quad [1]$$

where N_s is the total number of phase-encoding lines (i.e. shots or segments) in the full FOV distortion-free image, and

$$\Delta(s) = \Delta f(s)/BW_{px} = \Delta f(s)/\left(BW_{imaging}/N_y\right), \quad [2]$$

is the maximum pixel deviation along the EPI-PE coordinate. This results from off-resonance frequencies $\Delta f(s)$ induced by magnetic field inhomogeneities[4] and eddy-current effects[8] and is subject to the pixel bandwidth BW_{px} in the EPI-PE coordinate. In conventional EPI, this deviation manifests as geometric distortion (and modest inter-pixel

blurring). Note that N_s and N_y are assumed to be equal in the PSF mapping approach.[4] For a given imaging bandwidth $BW_{imaging}$, which is in turn determined by echo spacing Δt_{esp} and parallel imaging factor PI, and the maximum off-resonance bandwidth $\Delta f(s)_{max}$ corresponding to the maximum pixel deviation $\Delta(s)$ from the negative to the positive, the maximum available rFOV factor can be shown to be:[3]

$$rFOV_{max} = BW_{imaging}/\Delta f(s)_{max} = \left(PI/\Delta t_{esp}\right)/\Delta f(s)_{max}. \quad [3]$$

The reduced effective echo spacing of the DIADEM data is the main contributor to achieve a higher rFOV factor, which can be controlled by a parallel imaging factor and echo spacing, as shown by Eq. 3. A high gradient slew-rate is key to shorten the echo-spacing Δt_{esp}.[13] The reduced echo-spacing, along with increasing the imaging BW in the EPI-PE dimension, can further reduce the number of segment (i.e. the FOV) for the DIADEM acceleration in a given off-resonance bandwidth:

$$N_{seg,\ min} = N_s/rFOV_{max}. \quad [4]$$

Measurements of off-resonance frequency range in human brain on 3T MRI scanner

In order to apply a suitable maximum rFOV factor for the DIADEM acceleration in a certain imaging protocol, information about the total off-resonance bandwidth should be known, as suggested by Eq. 3. Therefore, the range of off-resonance frequencies at 3T was determined by a conventional dual-echo field mapping approach[16] on a standard whole-body (MR750, GE Healthcare, Chicago, IL, USA) and the compact 3T scanner. Data from 12 subjects were obtained on the whole-body scanner, and from 24 subjects on the compact 3T scanner, under an IRB-approved protocol. Written informed consent was obtained from all subjects. The imaging parameters for the field mapping were TR = 10.1/9.3 ms (whole-body/compact 3T), TE_1/TE_2 = 3.9/6.2 ms, flip angle (FA) = 10°, matrix size = 256×128, 38 slices, and slice thickness = 4 mm.

The image-processing steps using FSL toolkit (http://fsl.fmrib.ox.ac.uk/fsl/) proposed in a previous study[17] was followed in this study in order to investigate the frequency range from the field map measured within the brain, which included phase unwrapping, brain extraction, and alignment to the MNI (Montreal Neurological Institute) template in a standard space.[18] After converting the phase map to the frequency map, a search was conducted for the range of frequency values for each individual and for the entire group within the masked brain volume. In addition, the mean and the standard deviation maps for the entire group also were calculated.

Diffusion quality control phantom scan

DIADEM-based, quantitative diffusion imaging was evaluated using a diffusion quality control phantom (HPD Devices, Boulder, CO), as demonstrated in previous multi-site/multi-scanner studies.[19] The phantom was scanned with single-shot EPI and DIADEM at isocenter on the compact 3T scanner. After image reconstruction, gradient nonlinearity correction[20–22]

was additionally applied to minimize the bias in quantitative diffusion measurements due to gradient nonlinearity effects on the compact 3T. Finally, apparent diffusion coefficient (ADC) values were quantified from the center and inner vials containing the polymer polyvinylpyrrolidone (PVP) of 0%, 10%, 20%, 30%, 40% and 50% in the center slice. A circular region of interest (ROI), which had 1.72 cm diameter and included 317 voxels, was placed on each vial for the mean and standard deviation calculation.

Multi-band DIADEM sequence implementation and modification

The DIADEM diffusion sequence[3] combined with multi-band imaging[23,24] was implemented as shown in Fig. 1. To further minimize the scan time, a four-fold reduction in the navigator data acquisition window covering the center of k-space was additionally applied to yield lower-resolution navigator data. This is equivalent to assuming that the bandwidth of the spatial variation is smaller than 25% of the imaging bandwidth in the EPI-PE dimension. Due to the identical echo spacing used in the navigator, the level of image distortion in the signal acquisition was identical to the navigator data, which was important for providing robust, shot-to-shot motion-induced phase correction.

Experiments

To demonstrate the benefit of high-performance gradients, single-shot EPI-based high-resolution diffusion imaging was acquired on both the standard whole-body 3T with 50 mT/m gradient amplitude and 200 T/m/s slew-rate and the compact 3T operating at maxima of 80 mT/m and 700 T/m/s. The results were then compared with the proposed DIADEM approach on the compact 3T. Given maximum off-resonance bandwidth determined by the field mapping approach described above, diffusion quality control phantom and in-vivo experiments were conducted on the compact 3T to explore the highest in-plane and isotropic resolution for DIADEM diffusion imaging under three conditions including: i) 7 volumes with one and six b-values of 0 and 1000 s/mm^2, respectively that are the minimum requirements for diffusion tensor imaging (DTI) calculations, ii) entire brain volume coverage, and iii) obtainable in less than 10 minutes, our limit for a clinically feasible sequence. After that, the scan time reduction was tested by the reduction of the navigator echo acquisition window and with multi-band imaging. Along for DIADEM diffusion imaging, the conventional diffusion and anatomical imaging optimized for ongoing clinical studies at our institution were also performed for comparisons. Single-shot EPI was used for the conventional diffusion imaging. The anatomical imaging for this study included T2-weighted two-dimensional (2D) fast-spin-echo (FSE), 2D fluid-attenuated-inversion-recovery (FLAIR), and T1-weighted 3D magnetization prepared rapid acquisition gradient echo (MPRAGE). Eight volunteers (six normal controls and two patient subjects with brain tumors) were scanned using an 8-channel brain coil (Invivo, Gainesville, FL, USA) and a 32-channel brain coil (Nova Medical, Wilmington, MA, USA) on the compact 3T. Details of the imaging protocols are listed in Table 1. For all the scans performed on the compact 3T, artifacts due to linear and spatially independent concomitant fields were minimized by gradient pre-emphasis[25] and frequency tracking,[26] respectively.

After collecting DIADEM diffusion raw data, off-line reconstruction was performed using MATLAB (MathWorks, Natick, MA, USA). The DIADEM acquisition is essentially the

same as multi-shot and multi-echo (i.e. two-echo) EPI acquisition, but with and without additional SW-PE gradients, respectively, for the signal and the navigator echo acquisitions. Therefore, a vendor-provided, multi-band EPI image reconstruction was applied to separate the simultaneously excited slices in both the acquisitions. After the EPI reconstruction, DIADEM reconstruction[3] was followed based on the separated single-slice DIADEM data. Compared to the previous reconstruction pipeline[3], an off-resonance frequency offset of 50 Hz was considered during the distortion-free image calculation from the DIADEM data in order to account for an asymmetrical off-resonance frequency range often observed from human brains. For example, an offset of 50 Hz in the proposed reconstruction routine can cover from −200 to 300 Hz, rather than ±250 Hz range. After the rigid-body motion correction of the reconstructed DW images, DTI scalars including fractional anisotropy (FA), ADC, and color-coded FA were calculated using FSL (http://fsl.fmrib.ox.ac.uk/fsl/). In addition, a distortion map in the non-distorted space was calculated from the DIADEM data using the conventional PSF mapping approach[10] and converted to the corresponding off-resonance frequency map using Eq. 2. The map was used to quantitatively evaluate the level of distortion in EPI scanned for comparison.

Statistical Analysis

As a statistical method, Bland-Altman plot analysis[27] was applied to describe agreement between two approaches for quantitative ADC measurement. ADC agreements between EPI and DIADEM and between single-band and multi-band DIADEM were investigated in phantom and in-vivo experiment, respectively.

A pair of ADC volumes from the single-band and multi-band DIADEM data was compared in white matter areas over the entire brain. Due to its thicker slice thickness of 4 mm, there are expected to be strong partial volume effects of the ADC values anywhere close to CSF regions. To avoid these areas, the comparison was performed only in regions with FA values greater than 0.4 and ADC values less than 10×10^{-4} mm^2/s.

RESULTS

Off-resonance frequency range in human brain on 3T MRI scanner

Figure 2 shows the off-resonance frequency range on the standard whole-body and the compact 3T scanners observed in each individual subject, and for the entire group, within the human brain mask in the standard space. The maximum off-resonance range was similar on both the whole-body and the compact 3T scanners with default first-order (i.e., gradient) shimming. The total ranges were from −178.9 to 315.6 Hz and from −175.2 and 300.1 Hz, respectively on the whole-body and the compact 3T scanner. For each group, the mean and standard deviation of the maximum negative and positive frequency values on the whole-body scanner were −145.81±28.1 and 247.81±44.7, respectively. These values compared to −121.2±26.7 and 248.5±31.6 on the compact 3T. In addition, a linear trend of off-resonance frequency was observed along the slice (or physical Z) direction, as shown in the averaged off-resonance map (Fig. 2d).

Comparison of diffusion imaging with EPI and DIADEM

Figure 3 demonstrates that quantitative ADC values of the EPI and the proposed approach are well-matched. In distinction to the proposed approach, considerable susceptibility-induced geometric distortion was observed in EPI-based diffusion imaging. Despite the distortion in EPI images, all of ADC values with different PVP concentrations were very similar from both imaging methods (right top). This is because the distortion in EPI was identical over all diffusion data, and that the geometry mismatch between diffusion data caused by eddy-currents of diffusion gradients caused an observable ADC bias near the boundaries of the vials, but not in the homogeneous areas, which therefore did not affect the ADC measurements. However, the residual Nyquist ghosts due to imperfect Nyquist correction varied across the non-DW and DW images, but also in different locations. Furthermore, while the readout acquisition window could be shortened by a reduced resolution (rR) factor in the proposed approach, a longer readout acquisition window was required even with a partial Fourier factor of 5/8 (i.e. 22 vs. 54 echo train length, Table 1), which resulted in stronger Nyquist ghosts in single-shot EPI-based high-resolution imaging (Fig. 3). These produced a slight variation of ADC in both methods, but with different levels (see 4^{th}, 6^{th}, and 7^{th} vial results). Nevertheless, all of mean ADC values were within the 95% confidence interval in the Bland-Altman plot (right bottom) and were comparable to the result from a previous study.[19]

Geometric distortion in single-shot EPI-based high-resolution DW image was effectively reduced by employing the high-performance gradients on the compact 3T, as demonstrated in Fig. 4. Using a parallel imaging acceleration factor of 3 and the maximum gradient performance of 700 T/m/s slew-rate and 80 mT/m gradient amplitude, a much shorter effective echo spacing of 214.7 μs was obtained on the compact 3T, even with a high in-plane imaging matrix of 256×256 (Figs. 4b and 4c). This compares to the 352.0 μs that could be achieved on a standard, whole-body scanner with 50 mT/m gradient amplitude and 200 T/m/s gradient slew-rate. In addition, the shorter readout acquisition time on the compact 3T reduced geometrical distortion and T2 weighting (Fig. 4b), compared to the whole-body scanner (Fig. 4a). The off-resonance map calculated from the DIADEM data was able to cover a total off-resonance frequency range of ±296.6 Hz and the coverage ranged from −241 to 352.2 Hz after using an offset of 55.6 Hz (i.e. 18.52 Hz/pixel × 3 pixels) suggested in the proposed reconstruction. Therefore, it was sufficient to cover the maximum off-resonance frequency of up to 237 Hz shown in the temporal lobe of the brain (Fig. 4d). However, the level of distortion up to 13 pixels (11.2 mm) was still severe in regions of high susceptibility with the single-shot acquisition, especially for very high-resolution imaging, which resulted in a loss of spatial resolution in the affected areas (see white arrows in the color-coded FA map of Fig. 4b). For in-vivo imaging, eddy-current-induced geometric distortions due to diffusion encoding gradients also resulted in errors during the calculation of DTI scalars (yellow arrows in Figs. 4a and 4b). Note that these issues were not present when the proposed approach was used (Fig. 4c).

Highest in-plane and isotropic resolution within a clinically-feasible scan time on the compact 3T

As shown in Figure 5, the proposed diffusion approach is capable of producing virtually distortion-free high in-plane resolution images, comparable to those obtained in conventional 2D anatomical imaging, within a clinically-feasible scan time. Due to the short effective echo spacing of 209.3 μs on the compact 3T and an in-plane acceleration factor of 3, the acquisition with a rFOV factor of 8 covered a total off-resonance range of ±298.6 Hz (Eq. 3). Since the range is wider than that of in-vivo human brain shown in Fig. 2, there was no observable wraparound artifacts in the reconstructed images (Figs. 5a and 5b). In addition, using a 9:46 minute scan time, it was possible to achieve a maximum in-plane resolution of up to 0.86 mm^2 with a 4 mm thickness and 38 slice coverage, which is equivalent to the protocols for conventional 2D anatomical imaging including FSE (Fig. 5e) and FLAIR (Fig. 5f). Therefore, the coverage and image resolution of the diffusion and anatomic imaging are well-matched. The scan time was further reduced to 8:10 minutes after the reduction of the navigator echo acquisition window, without sacrificing reconstructed image quality.

Figure 6 shows the proposed whole brain diffusion imaging with an isotropic resolution of 1.4 mm^3. A rFOV factor of 13 resulted in 12 shots for each DIADEM scan, according to Eq. 4. With an effective echo spacing of 145.3 μs, the off-resonance frequency range covered up to ±264.6 Hz. By applying a partial Fourier factor of 83.3% in the SW-PE dimension, it was possible to reduce the total number of shots from 12 to 10 for each DIADEM acquisition. As shown in the sagittal plane images, the proposed distortion-free approach provided a substantial improvement in image quality, especially near the frontal lobes and midbrain areas. The scan time was also reduced from 9:37 to 8:36 after the reduction of the navigator echo acquisition window.

Implementation of multi-band DIADEM

Figure 7 presents comparison of color-coded FA maps between single-band and multi-band DIADEM. When compared to the single-band imaging, multi-band imaging resulted in generally similar image quality, while the scan time was reduced from 8:10 to 5:11 using a multi-band factor of 3. As shown in color-coded vector map overlaid on the FA map (Figure 7, third column), similar patterns can be seen in the vector maps obtained from both single-band and multi-band imaging. Although only six diffusion directions were applied in both imaging, the cortical diffusion anisotropy entering the cortex to be perpendicular to the cortical surface and its radial diffusion orientation are clearly visible.

Figure 8 shows a comparison between the ADCs obtained from single-band and multi-band DIADEM imaging of the human brain. Visual inspection of the images suggests that the multi-band DIADEM data are very similar to the single-band data. As shown in the histogram (top and 3rd column) and Bland-Altman plot (bottom row) of the ADC differences that were calculated in white matter areas over the entire brain, the ADC differences showed negligible bias and trend throughout the range of ADC measurement. In addition, the results were very consistent over all four subjects.

Brain tumor diffusion imaging using DIADEM

Figure 9 illustrates the potential benefit of the proposed distortion-free imaging for use in clinical diagnosis. Although anatomical details can be observed in the conventional EPI-based high-resolution imaging, it suffered from geometric distortion. As image stretching and pile-up, the maximum geometric distortion of up to 17.7 pixels (equal to 15.2 mm) appeared in regions of high susceptibility, even when the compact 3T was used (Figs. 9a-b). The spatially varying residual distortions resulted in unclear boundaries or ambiguity around the brain tumor near areas of rapid susceptibility variation (see red arrows in Figs. 9a and 9g). In distinction, the proposed high-resolution DIADEM provided a high degree of anatomic detail, without any observable artifacts since this acquisition could yield a distortion-free image from the DIADEM data without fold-over artifacts within the off-resonance frequency range from −242.6 to 354.5 Hz. This permitted the brain tumor to be readily characterized, even near areas of rapid susceptibility variation adjacent to tissue-air interfaces (Fig. 9, bottom row).

Figure 10 shows the mass effect of a brain tumor. The tumor had a diameter of up to 2.73 cm and was sufficiently large to deform and displace the brainstem (Fig. 10a). The effects could be clearly observed in high spatial resolution diffusion images and corresponding DTI scalars in regions adjacent to the tumor. As shown in high anisotropic diffusion (Fig. 10d) and the direction (Fig. 10e), white matter tracts were displaced by the tumor. The differences were more apparent than in the corresponding areas in the healthy volunteer measured with an identical resolution (Fig. 10f).

DISCUSSION

In this study, an effective approach for high-resolution distortion-free diffusion imaging, termed DIADEM, was optimized based on a novel compact 3T system, and adapted for clinical applications. Utilizing the high gradient performance of a compact 3T system in conjunction with improvements to the imaging methods, the proposed approach allows high-resolution, distortion-free, whole-brain diffusion imaging within a clinically-feasible scan time of 5–10 minutes. This potentially enables one-to-one image matching with conventional 2D anatomical images and diffusion for clinical usage. These preliminary results demonstrate the superiority of the method over the conventional diffusion approach in characterizing brain tumors, especially near regions with rapid susceptibility variation.

Conventional B0 field mapping[16] was performed in order to measure the off-resonance frequency range in the human brain in an attempt to systemically search for a reasonable maximum rFOV factor for the DIADEM scan acceleration on the compact 3T. The total off-resonance bandwidth to cover the entire brain volume, as measured on 36 subjects, was approximately 500 Hz. Since the proposed DIADEM acquisitions covered 597.2 and 524 Hz ranges, respectively, for high in-plane and isotropic resolution, wraparound artifacts caused by a high rFOV reduction in the SW-PE dimension were avoided. However, the off-resonance frequency range determined in this study may not fit all clinical scenarios, since the range may not be valid in patients with metallic implants that typically generate greater field distortions (or off-resonance frequency). To accurately cover an atypical off-resonance

range, either the conventional field mapping[16] or PSF mapping approach[10,28] will be needed before applying the proposed approach to those wider clinical scenarios.

Compared to a conventional 3T MRI system, an approximately 2.5-fold faster scan time of EPI was achieved on the compact 3T due to the benefit of high-performance gradients for sub-millimeter in-plane resolution diffusion imaging. In high in-plane resolution diffusion imaging using DIADEM, the use of a high slew-rate gradient shortened the echo spacing by 40%, which allowed a maximum rFOV factor of 8 for the DIADEM acceleration, higher than the maximum of 5 that was applied previously.[3] In addition, the high gradient slew-rate and amplitude decreased both the entire readout duration as well as the diffusion encoding time, resulting in a much shorter TR, which further reduces the scan time. In general, high rFOV acceleration leads to a lower averaging in an acquisition, and reduces the overall SNR in the reconstructed image. Nevertheless, a high number of shots corresponding to 27 and 10 were applied for high in-plane (0.86 mm^2 with a 4 mm slice thickness) and isotropic (1.4 mm^3) resolution diffusion imaging, respectively. This demonstrated small anatomical features using DIADEM.

The 4-fold reduction in navigator echo data acquisition resulted in an up to 17% reduction in TR, and thus the total scan time in the DIADEM acquisition since gradient-echo-type rather than spin-echo-type 2D navigator echo data[29] was collected. Although the time-shortened navigator echo data may not include high-order spatial components induced by involuntary motion, we noticed that the high-performance gradients at least partially compensated for this problem. Since involuntary motions during the diffusion encoding can cause dominant phase errors between shots,[5–7] the shorter diffusion encoding with the high-performance gradient could reduce the errors in the data acquisition. Furthermore, the minimized TE for the navigator echo data acquisition (less than 60 ms) could potentially increase the SNR, thus improving the reliability in calculating the phase error. Finally, the increased imaging PE BW due to a high gradient slew-rate could accommodate even higher-order spatial components induced by involuntary motions. Therefore, we expect that reasonable motion-induced phase correction could be readily achieved on the compact 3T.

Further scan time reduction of up to 36% was achieved with multi-band imaging. To obtain the scan time reduction, MB-DIADEM data were slightly noisier than the SB-DIADEM data. However, it was still possible to obtain FA and ADC maps using MB-DIADEM scans that were comparable to those obtained from SB-DIADEM data. The scan time reduces to 3 minutes when only the ADC measurement is required. In addition, the scan time reduction could be useful for making this approach clinically available even with conventional gradient performance, as well as to extend to DTI applications on the compact 3T scanner that require more diffusion directions rather than six applied in this study.

The proposed approach allows reliable ADC measurements, as demonstrated by diffusion quality phantom scan. When compared to single-shot EPI and the results performed previously,[19] all of measured ADC values with different PVP concentrations from 0% to 50% were within the acceptable range of difference. This demonstrates the reliability of the ADC measurements, since the entire range covers the ADC values in white matter and gray matter of human brain. Comparable ADC measurement was possible even with the multi-

band imaging, without introducing noticeable artefact or bias. Visual inspection of the histogram of the ADC difference suggested that the overall range of the ADC difference was similar to that observed in a previous study[30] demonstrated with readout-segmented EPI (see Fig. 2 in Frost et al.[30]). While the accuracy of quantitative diffusion measurement in EPI was not affected by distortions on the homogeneous phantom, this would be problematic in in-vivo imaging due to the complex structure of the brain, as demonstrated in the FA maps. Therefore, the proposed approach without suffering from EPI distortions will be a reliable tool for quantitative diffusion imaging in in-vivo.

High-resolution diffusion imaging using the conventional single-shot EPI acquisition and basic inverse Fourier and linear parallel imaging reconstruction (conventional) was still suboptimal, even after the considerable improvements from the high-performance gradients on the compact 3T. The maximum spatial distortion of high-resolution images measured on the compact 3T scanners were 15.2 mm in this study. There were also additional loss of spatial resolution in EPI-based high-resolution imaging due to severe T2* blurring, which increased linearly with the readout acquisition window duration, and varying eddy-current-induced distortions resulting in image mismatch between the DW images. In distinction, the proposed approach can clearly mitigate these drawbacks, and the prolonged scan time was reduced with the high-performance gradients and multi-band imaging. Substantially improved high-resolution diffusion imaging was demonstrated on the compact 3T only with a 2.4 times longer scan time than a single-shot EPI on the standard whole-body scanner. Therefore, the improvements in both hardware and imaging sequence represent an effective strategy to address the challenges to obtain high spatial resolution diffusion image with good image quality.

The proposed approach enables a direct one-to-one image comparison between diffusion and the anatomical images for clinical evaluation due to the matching image resolution and geometry. The accuracy of image geometry matching could be particularly important in terms of the image-based quantification of diffusion data, since any geometric distortion in EPI would result in errors during the calculation in the ROI drawn on anatomical images. With the proposed high-resolution diffusion approach, detailed and reliable anatomic information can be achieved, even in areas that are adjacent to the paranasal sinuses, the eyes, and tissue/air boundaries, where strong susceptibility effects typically appear. Although these preliminary results on the compact 3T appear to be promising for patients with brain tumors compared to EPI, they should be considered preliminary, and further investigation is still necessary.

In this work, single-shot EPI and the proposed method (DIADEM) were compared in terms of their ability to efficiently collect MRI data that are visually unaffected by common non-idealities like susceptibility variation and eddy-currents. Due to DIADEM's efficient encoding strategy, distortion-free images can be generated from DIADEM data without processing that requires explicit knowledge of off-resonance fields. For single-shot EPI, that information is typically obtained from separate calibration scans,[8,16] jointly estimated during image reconstruction[31] or retrospectively estimated during post-processing of distorted reconstruction results,[8,16,32] all of which are numerically sensitive and/or computationally intensive processes. Having said this, images could also be generated from

data acquired via the proposed DIADEM sequence using model based iterative reconstruction (MBIR),[33] which is expected to provide even greater gains in image quality by robustly accounting for image discretization effects as well as enabling use of advanced image prior models like compressed sensing.[34] Due to the inherent redundancies in DIADEM encoding, the relative advantages of MBIR for DIADEM are expected to at least meet – and likely exceed – those recently demonstrated for single-shot EPI.[35] This line of activity will be investigated in a separate, future work.

Like all MRI pulse sequences, the proposed DIADEM acquisition strategy is subject to gradient nonlinearity effects, which cause geometric distortions in all types of structural imaging if not properly accounted for. As the sources of these distortions are both understood and well-characterized, they can be almost completely corrected either during image reconstruction,[36–38] or by interpolation in the image domain after image reconstruction.[39] Beyond applications where geometric accuracy is critical (e.g., radiation therapy planning), gradient nonlinearity also results in spatially dependent b-values leading to high non-uniformity errors in measurements of DTI scalars in diffusion imaging applications.[20,22,40] In this work, the gradient non-uniformity correction was applied in phantom experiment only for evaluation of quantitative diffusion measurements. In the future, therefore, both corrections should be fully integrated into the proposed approach to accurately quantify the DTI scalars in the targeted ROI area.

In this study, the DTI calculation was performed by using the minimal number of the DW volumes (i.e. six) and mainly with high in-plane anisotropic rather than isotropic resolution. In FA estimation, however, an acquisition of more than thirty diffusion directions[41] is often preferred to improve accuracy, and the anisotropic voxel size can affect the measured FA value, especially in regions of the brain with crossing fibers.[42] Therefore, further evaluation for quantitative diffusion measurements would be required using the proposed approach with an isotropic resolution and high number of diffusion directions. Due to the reduced imaging coverage of the compact 3T MRI system compared with conventional whole-body clinical MRI systems, the improvements are applicable only for brain and extremities (e.g., wrists, knees, feet) applications.[12]

We reported the potential clinical use of a DIADEM approach on a compact 3T scanner for the diffusion imaging of brain tumors through the use of high-performance gradients and sequence developments. Since this approach is virtually immune to off-resonance-induced distortions as well as T2* blurring that are generally observed with single-shot EPI, the multi-shot nature of this approach enables high spatial resolution diffusion imaging, substantial improvements in characterizing brain tumors can be achieved in areas of high susceptibility. In addition, it was demonstrated that reliable ADC measurements were possible even in high-resolution diffusion imaging combined with multi-band imaging. With the high spatial resolution capability, the proposed approach can be particularly useful for evaluating brain tumors and surrounding structures in regions that are vulnerable to susceptibility artifacts such as the skull base.

Acknowledgments:

Authors wish to thank Drs. Brice Fernandez and Dan Rettmann from GE Healthcare for sharing the source code of the multi-echo EPI.

Grant Support:

This work was supported by NIH U01 EB024450-01.

REFERENCES

1. Le Bihan D, Breton E. Imagerie de diffusion in-vivo par résonance magnétique nucléaire. Comptes-Rendus de l'Académie des Sciences. 1985;93(5):27–34.
2. Holodny AI, Ollenschlager M. Diffusion imaging in brain tumors. Neuroimaging Clinics. 2002;12(1):107–124. [PubMed: 11998248]
3. In MH, Posnansky O, Speck O. High-resolution distortion-free diffusion imaging using hybrid spin-warp and echo-planar PSF-encoding approach. NeuroImage. 2017;148:20–30. [PubMed: 28065851]
4. Robson MD, Gore JC, Constable RT. Measurement of the point spread function in MRI using constant time imaging. Magn Reson Med. 1997;38(5):733–740. [PubMed: 9358447]
5. Holdsworth SJ, Skare S, Newbould RD, Guzmann R, Blevins NH, Bammer R. Readout-segmented EPI for rapid high resolution diffusion imaging at 3T. European journal of radiology. 2008;65(1): 36–46. [PubMed: 17980534]
6. Porter DA, Heidemann RM. High resolution diffusion-weighted imaging using readout-segmented echo-planar imaging, parallel imaging and a two-dimensional navigator-based reacquisition. Magnetic Resonance in Medicine. 2009;62(2):468–475. [PubMed: 19449372]
7. Chen N-K, Guidon A, Chang H- C, Song AW. A robust multi-shot scan strategy for high-resolution diffusion weighted MRI enabled by multiplexed sensitivity-encoding (MUSE). Neuroimage. 2013;72:41–47. [PubMed: 23370063]
8. In MH, Posnansky O, Speck O. PSF mapping-based correction of eddy-current-induced distortions in diffusion-weighted echo-planar imaging. Magnetic resonance in medicine. 2016;75(5):2055–2063. [PubMed: 26096666]
9. In MH, Speck O. Highly accelerated PSF-mapping for EPI distortion correction with improved fidelity. Magnetic Resonance Materials in Physics, Biology and Medicine. 2012;25(3):183–192.
10. Zaitsev M, Hennig J, Speck O. Point spread function mapping with parallel imaging techniques and high acceleration factors: Fast, robust, and flexible method for echo planar imaging distortion correction. Magn Reson Med. 2004;52(5):1156–1166. [PubMed: 15508146]
11. Lee SK, Mathieu JB, Graziani D, et al. Peripheral nerve stimulation characteristics of an asymmetric head-only gradient coil compatible with a high-channel-count receiver array. Magnetic resonance in medicine. 2016;76(6):1939–1950. [PubMed: 26628078]
12. Foo TK, Laskaris E, Vermilyea M, et al. Lightweight, compact, and high-performance 3 T MR system for imaging the brain and extremities. Magnetic resonance in medicine. 2018;80(5):2232–2245. [PubMed: 29536587]
13. Tan ET, Lee SK, Weavers PT, et al. High slew-rate head-only gradient for improving distortion in echo planar imaging: Preliminary experience. Journal of Magnetic Resonance Imaging. 2016;44(3):653–664. [PubMed: 26921117]
14. Tan ET, Hardy CJ, Shu Y, et al. Reduced acoustic noise in diffusion tensor imaging on a compact MRI system. Magnetic resonance in medicine. 2018;79(6):2902–2911. [PubMed: 28971512]
15. Weavers PT, Shu Y, Tao S, et al. Compact three-tesla magnetic resonance imager with high-performance gradients passes ACR image quality and acoustic noise tests. Medical physics. 2016;43(3):1259–1264. [PubMed: 26936710]
16. Jezzard P, Balaban RS. Correction for geometric distortion in echo planar images from B0 field variations. Magn Reson Med. 1995;34(1):65–73. [PubMed: 7674900]
17. Shi Y, Vannesjo SJ, Miller KL, Clare S. Template-based field map prediction for rapid whole brain B0 shimming. Magnetic resonance in medicine. 2018;80(1):171–180. [PubMed: 29193340]

18. Grabner G, Janke AL, Budge MM, Smith D, Pruessner J, Collins DL. Symmetric atlasing and model based segmentation: an application to the hippocampus in older adults. International Conference on Medical Image Computing and Computer-Assisted Intervention 2006;9(Pt 2):58–66.
19. Palacios EM, Martin AJ, Boss MA, et al. Toward precision and reproducibility of diffusion tensor imaging: a multicenter diffusion phantom and traveling volunteer study. American Journal of Neuroradiology. 2017;38(3):537–545. [PubMed: 28007768]
20. Malyarenko DI, Ross BD, Chenevert TL. Analysis and correction of gradient nonlinearity bias in apparent diffusion coefficient measurements. Magnetic resonance in medicine. 2014;71(3):1312–1323. [PubMed: 23794533]
21. Tan ET, Marinelli L, Slavens ZW, King KF, Hardy CJ. Improved correction for gradient nonlinearity effects in diffusion-weighted imaging. Journal of Magnetic Resonance Imaging. 2013;38(2):448–453. [PubMed: 23172675]
22. Tao AT, Shu Y, Tan ET, et al. Improving apparent diffusion coefficient accuracy on a compact 3T MRI scanner using gradient non-linearity correction. Journal of Magnetic Resonance Imaging. 2018;48(6):1498–1507. [PubMed: 30255963]
23. Setsompop K, Gagoski BA, Polimeni JR, Witzel T, Wedeen VJ, Wald LL. Blipped-controlled aliasing in parallel imaging for simultaneous multislice echo planar imaging with reduced g-factor penalty. Magnetic resonance in medicine. 2012;67(5):1210–1224. [PubMed: 21858868]
24. Zhu K, Dougherty RF, Wu H, et al. Hybrid-space SENSE reconstruction for simultaneous multi-slice MRI. IEEE transactions on medical imaging. 2016;35(8):1824–1836. [PubMed: 26915118]
25. Tao S, Weavers PT, Trzasko JD, et al. Gradient pre-emphasis to counteract first-order concomitant fields on asymmetric MRI gradient systems. Magnetic resonance in medicine. 2017;77(6):2250–2262. [PubMed: 27373901]
26. Weavers PT, Tao S, Trzasko JD, et al. B0 concomitant field compensation for MRI systems employing asymmetric transverse gradient coils. Magnetic resonance in medicine. 2017;79(3):1538–1544. [PubMed: 28639370]
27. Bland JM, Altman D. Statistical methods for assessing agreement between two methods of clinical measurement. The lancet. 1986;327(8476):307–310.
28. In MH, Cho S, Shu Y, et al. Correction of metal-induced susceptibility artifacts for functional MRI during deep brain stimulation. NeuroImage. 2017;158:26–36. [PubMed: 28666879]
29. Holdsworth SJ, Yeom K, Skare S, Gentles AJ, Barnes PD, Bammer R. Clinical Application of Readout-Segmented− Echo-Planar Imaging for Diffusion-Weighted Imaging in Pediatric Brain. American Journal of Neuroradiology. 2011;32(7):1274–1279. [PubMed: 21596809]
30. Frost R, Jezzard P, Douaud G, Clare S, Porter DA, Miller KL. Scan time reduction for readout-segmented EPI using simultaneous multislice acceleration: Diffusion-weighted imaging at 3 and 7 Tesla. Magnetic resonance in medicine. 2015;74(1):136–149. [PubMed: 25078777]
31. Sutton BP, Noll DC, Fessler JA. Dynamic field map estimation using a spiral-in/spiral-out acquisition. Magnetic Resonance in Medicine. 2004;51(6):1194–1204. [PubMed: 15170840]
32. Andersson JL, Skare S, Ashburner J. How to correct susceptibility distortions in spin-echo echo-planar images: application to diffusion tensor imaging. Neuroimage. 2003;20(2):870–888. [PubMed: 14568458]
33. Fessler JA. Model-based image reconstruction for MRI. IEEE Signal Processing Magazine. 2010;27(4):81–89. [PubMed: 21135916]
34. Lustig M, Donoho DL, Santos JM, Pauly JM. Compressed sensing MRI. IEEE signal processing magazine. 2008;25(2):72–82.
35. Yarach U, In MH, Chatnuntawech I, et al. Model-based iterative reconstruction for single-shot EPI at 7T. Magnetic resonance in medicine. 2017;78(6):2250–2264. [PubMed: 28185433]
36. Tao S, Trzasko JD, Shu Y, Huston J, Bernstein MA. Integrated image reconstruction and gradient nonlinearity correction. Magnetic resonance in medicine. 2015;74(4):1019–1031. [PubMed: 25298258]
37. Tao S, Trzasko J, Gunter J, et al. Gradient nonlinearity calibration and correction for a compact, asymmetric magnetic resonance imaging gradient system. Physics in Medicine & Biology. 2016;62(2):N18. [PubMed: 28033119]

38. Weavers PT, Tao S, Trzasko JD, et al. Image-based gradient non-linearity characterization to determine higher-order spherical harmonic coefficients for improved spatial position accuracy in magnetic resonance imaging. Magnetic resonance imaging. 2017;38:54–62. [PubMed: 28034637]

39. Glover GH, Pelc NJ. Method for correcting image distortion due to gradient nonuniformity. U.S. Patent No. 4,591,789; 1986.

40. Bammer R, Markl M, Barnett A, et al. Analysis and generalized correction of the effect of spatial gradient field distortions in diffusion-weighted imaging. Magnetic resonance in medicine. 2003;50(3):560–569. [PubMed: 12939764]

41. Jones DK. The effect of gradient sampling schemes on measures derived from diffusion tensor MRI: a Monte Carlo study. Magnetic Resonance in Medicine: An Official Journal of the International Society for Magnetic Resonance in Medicine. 2004;51(4):807–815.

42. Oouchi H, Yamada K, Sakai K, et al. Diffusion anisotropy measurement of brain white matter is affected by voxel size: underestimation occurs in areas with crossing fibers. American Journal of Neuroradiology. 2007;28(6):1102–1106. [PubMed: 17569968]

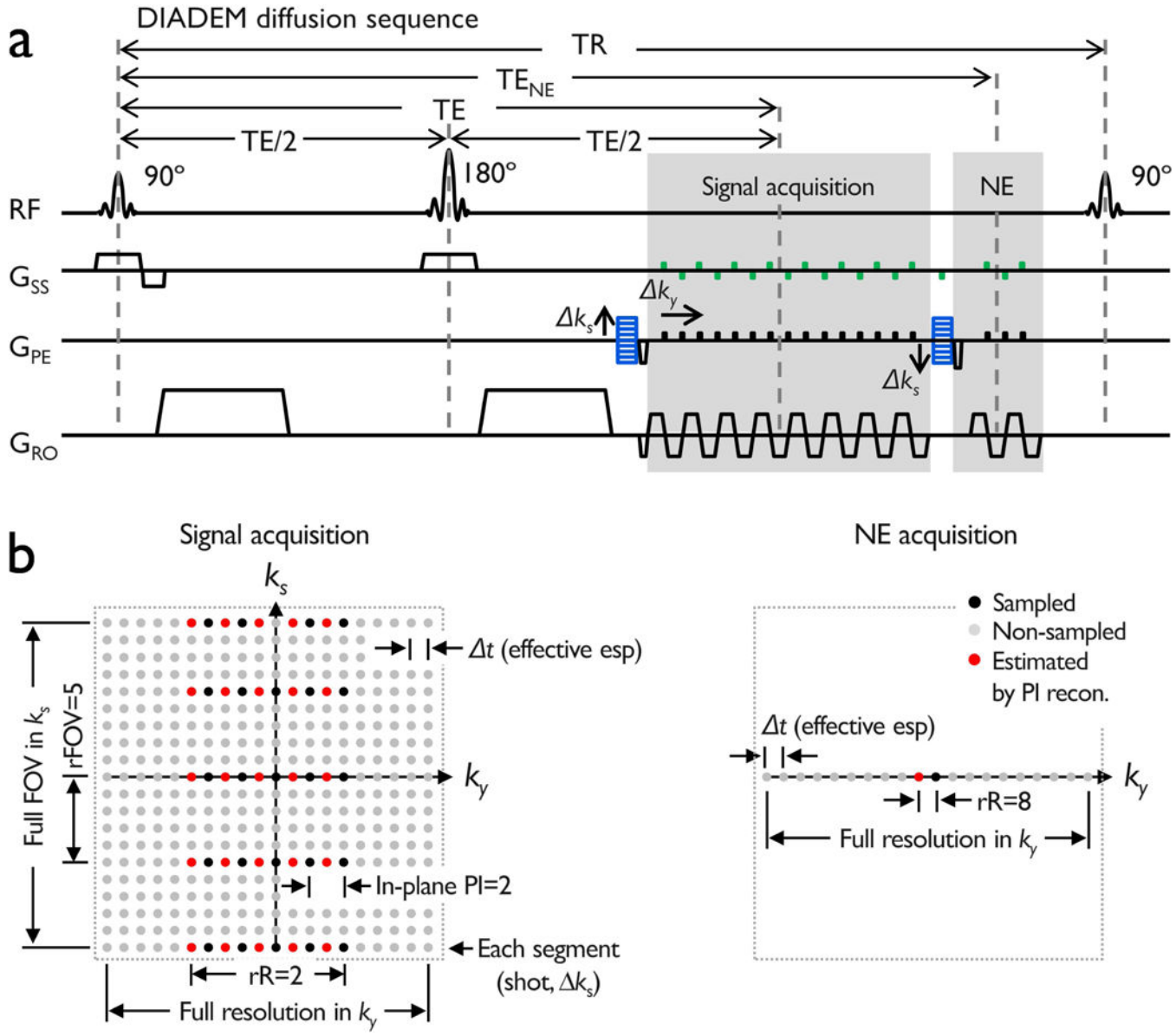

Figure 1.

A multi-band DIADEM diffusion sequence diagram with a navigator-echo (a) and corresponding k-space (b). The navigator-echo (NE) acquisition window is reduced by four times compared to the signal acquisition window. Note that spin-warp phase-encoded and corresponding rewinder gradients, see $\Delta k_{s,}$ (blue) are applied before and after the spin-warp phase-encoded signal acquisition,[3] and multi-band acquisition scheme (green) is added on the slice selection axis during the signal and the navigator echo acquisition. In (b), a summarized description of the k-space including the important dimensions and various parameters applied in this method is presented. The abbreviations are: FOV: field of view, rFOV: reduced FOV, rR: reduced resolution, esp: echo spacing, PI: parallel imaging.

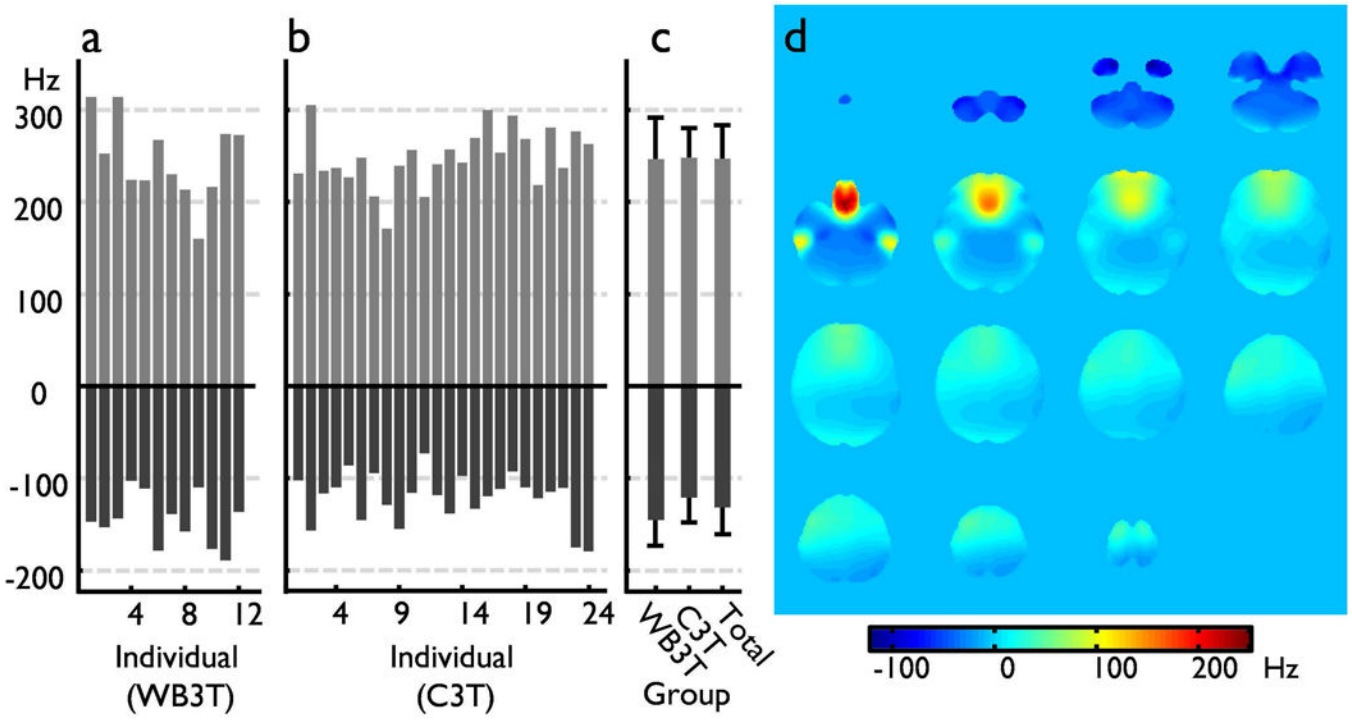

Figure 2.

The off-resonance frequency range within masked brain volume in the standard space. Each individual off-resonance range on the whole-body 3T (WB3T, a) and the compact 3T (C3T, b), and the group data (c) are shown. In addition, an averaged off-resonance frequency map for the data for the entire group, including C3T and WB3T data is presented in (d).

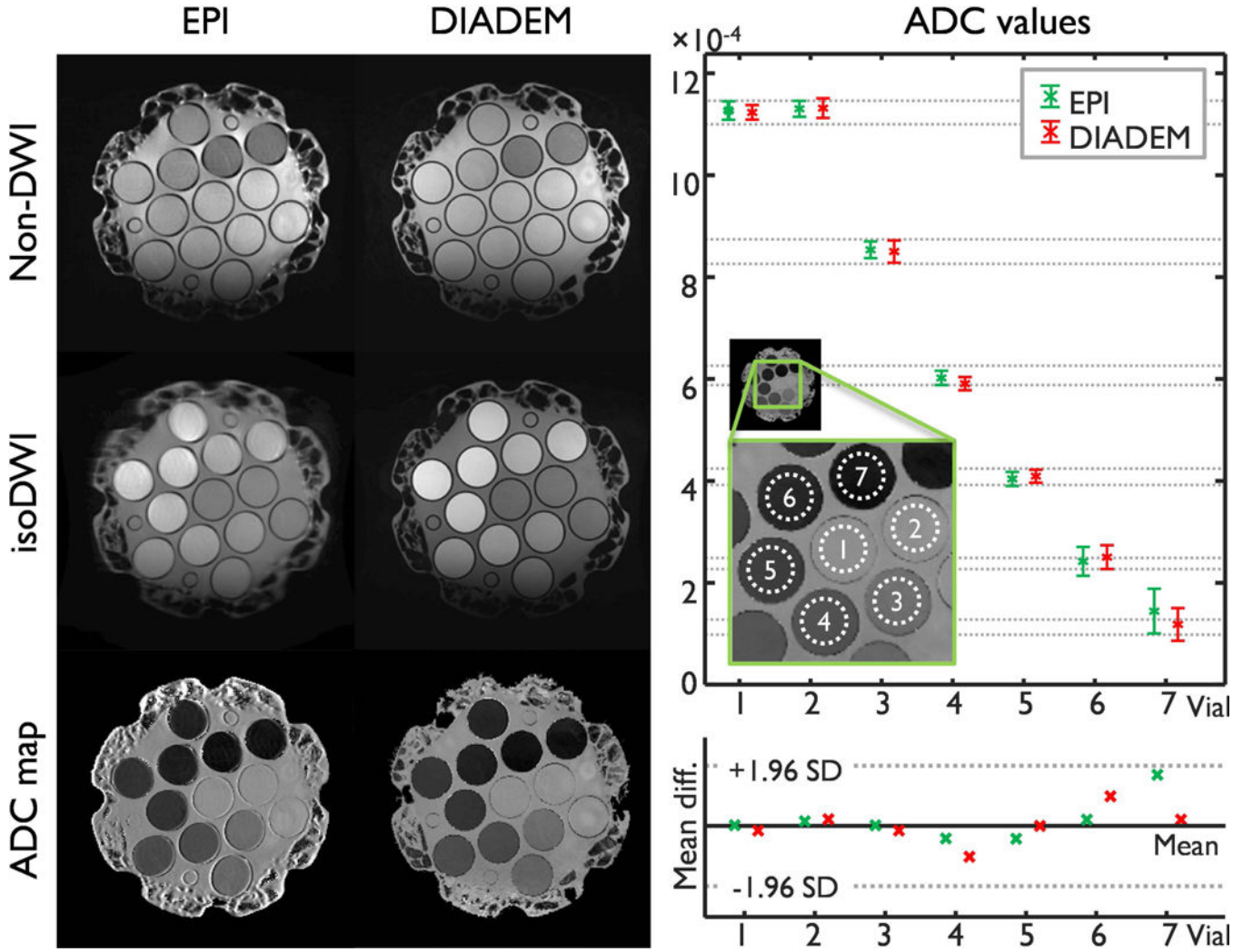

Figure 3.

Diffusion quality control phantom measurements using EPI and DIADEM: Non-diffusion weighted image (DWI) and sum of all 6 diffusion weighted images (isoDWI) and corresponding ADC map were shown in the left. The intrinsic (i.e., acquired) image resolution is 0.86×0.86×4 mm^3 (Table 1–5 and 1–8). On the right and top, the mean and standard deviation of ADC values measured from seven vials (shown in the zoomed image) were shown. Note that the seven vials from 1st to 7th contain the PVP of 0%, 0%, 10%, 20%, 30%, 40%, and 50%, respectively. As a reference, gray dashed lines show the standard deviation (SD) of ADC values measured on thirteen 3T MR scanners at 11 different sites in a previous study.[19] On the right and bottom, a Bland–Altman plot shows agreement of the mean ADC values in between this (i.e. both EPI and DIADEM) and the previous study.[19] The mean and the 95% confidence interval (±1.96 SD) lines were drawn based on the results from the previous study.[19]

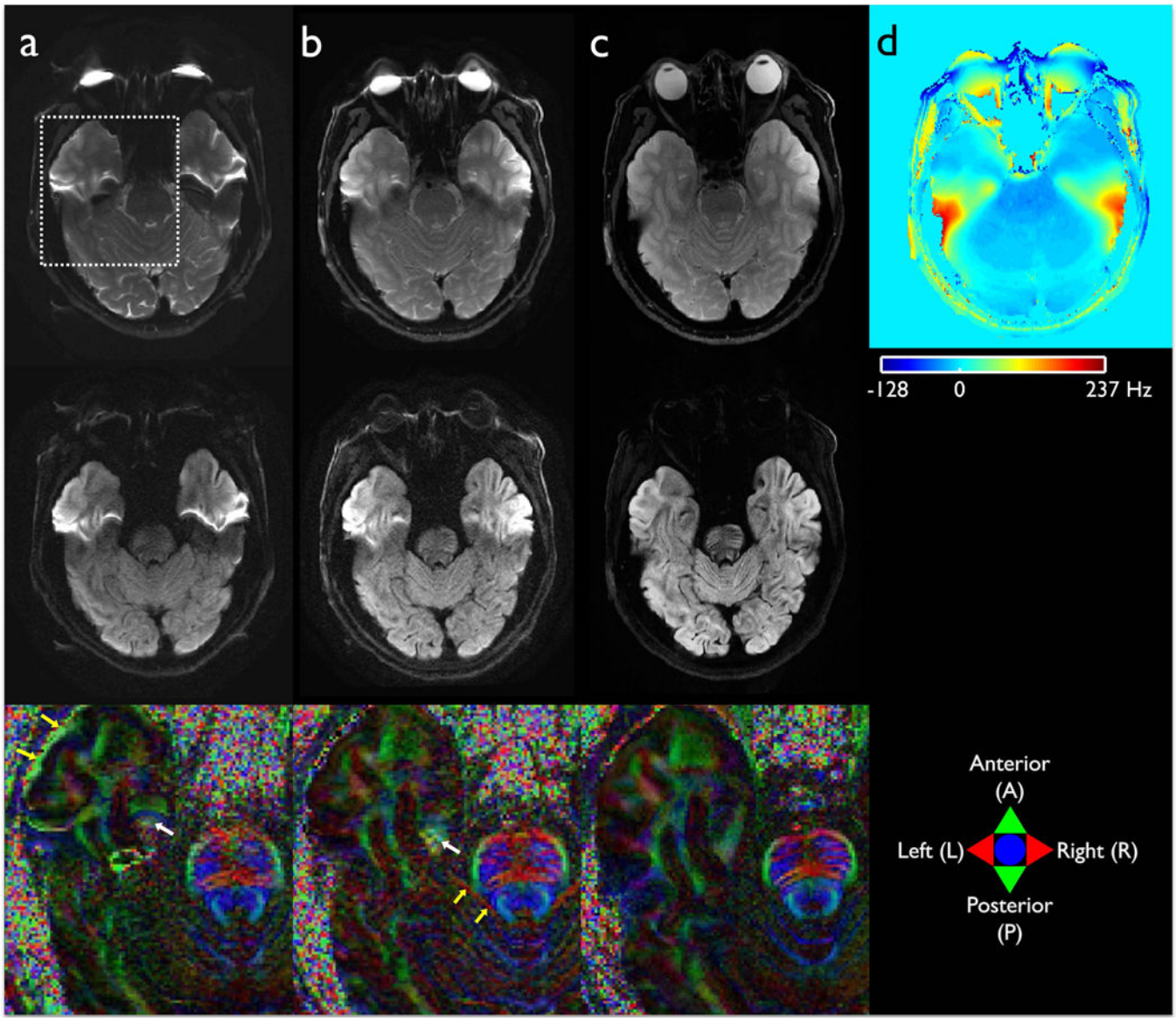

Figure 4.

High-resolution diffusion imaging on the standard whole-body (a) and the compact 3T MRI (b and c) acquired using single-shot EPI (a and b) and the proposed multi-shot DIADEM approach (c). The susceptibility-induced off-resonance effect during EPI and DIADEM acquisitions on the compact 3T are shown as a masked frequency map covering brain areas in (d). A slice from each non-DWI (upper), DWI image (middle), and color-coded FA map (bottom) enlarged from a dashed rectangular area shown in (a) was chosen for demonstration. In the color-coded FA maps (bottom row), green, red, and blue colors represent the dominant diffusion along the anterior-to-posterior (AP), right-to-left (RL), superior-to-inferior (SI) directions, respectively. Yellow and white arrows indicate the loss of spatial resolution caused by eddy-current- and susceptibility-induced geometric distortions. The intrinsic image resolution is 0.94(AP)×0.94(RL)×4(SI) mm^3 (Table 1–1-3).

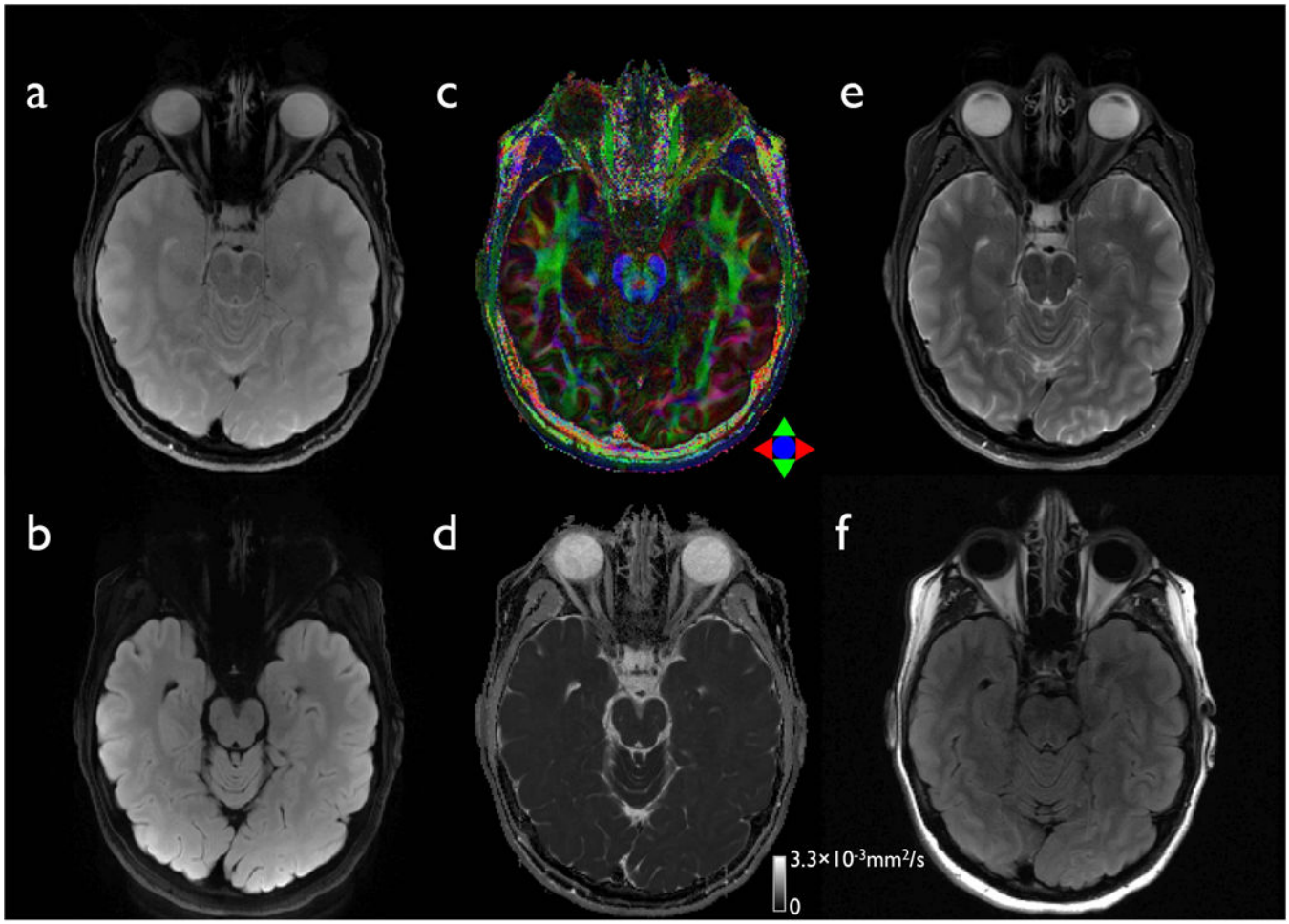

Figure 5.

The proposed diffusion (a-d) and conventional anatomical images (e-f) with a high in-plane resolution. A slice from non-DWI (a), isoDWI obtained by the summation of all 6 DWIs (b), color-coded FA map (c), and MD map (d) are displayed. The corresponding slices from the anatomical 2D-FSE (e) and FLAIR data (f) are shown for comparison. The intrinsic image resolution is 0.86×0.86×4 mm^3 for both diffusion (Table 1–5) and anatomical data (Table 1–9 and 1–10).

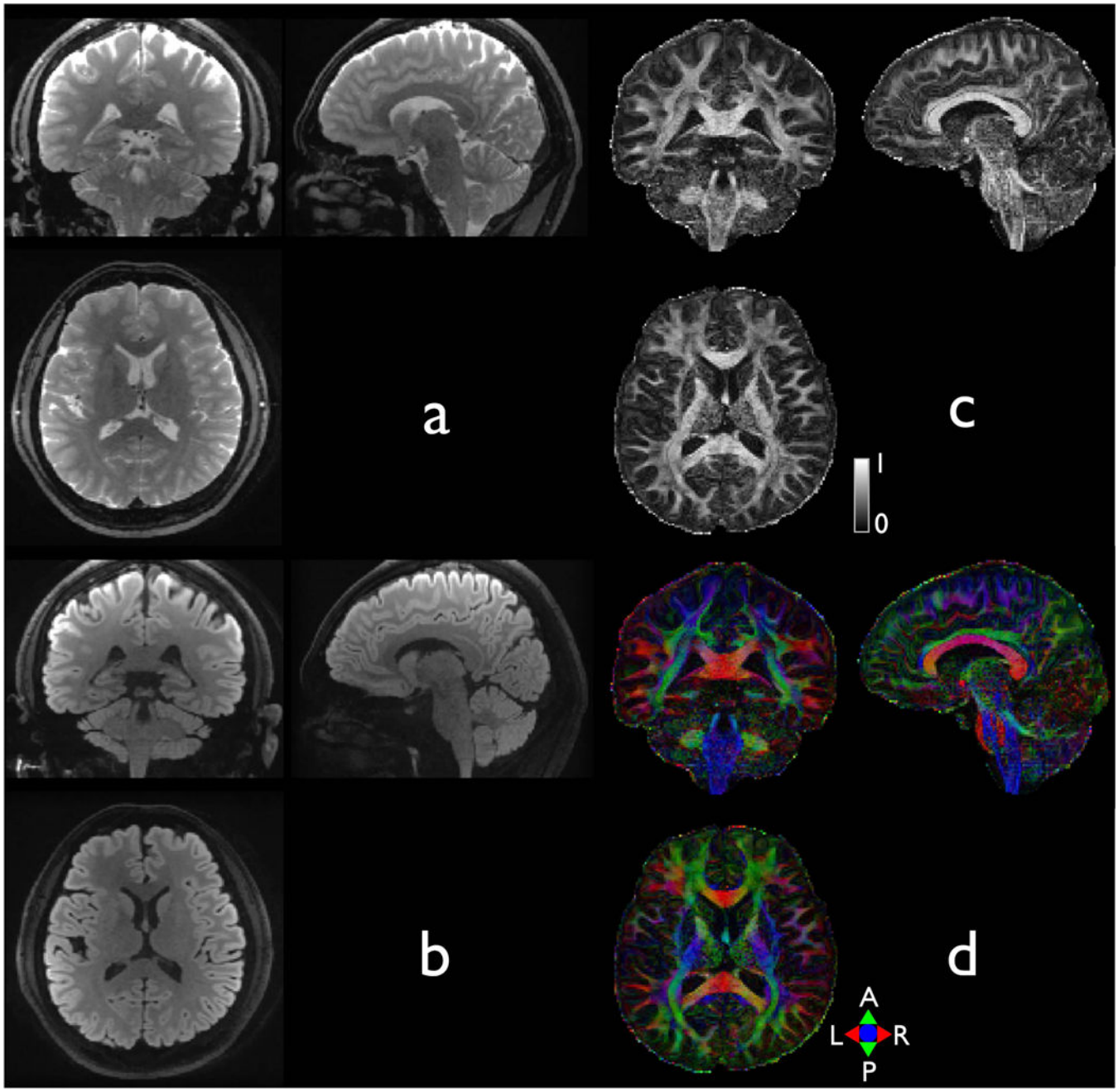

Figure 6.

Whole brain diffusion imaging with an isotropic resolution of 1.4 mm^3. For demonstration purpose, reformatted coronal, reformatted sagittal, and axial slices of non-DWI (a), isoDWI (b), FA (c), and a color-coded FA map (e) selected from a 3D brain volume. The imaging protocols are shown in Table 1–4.

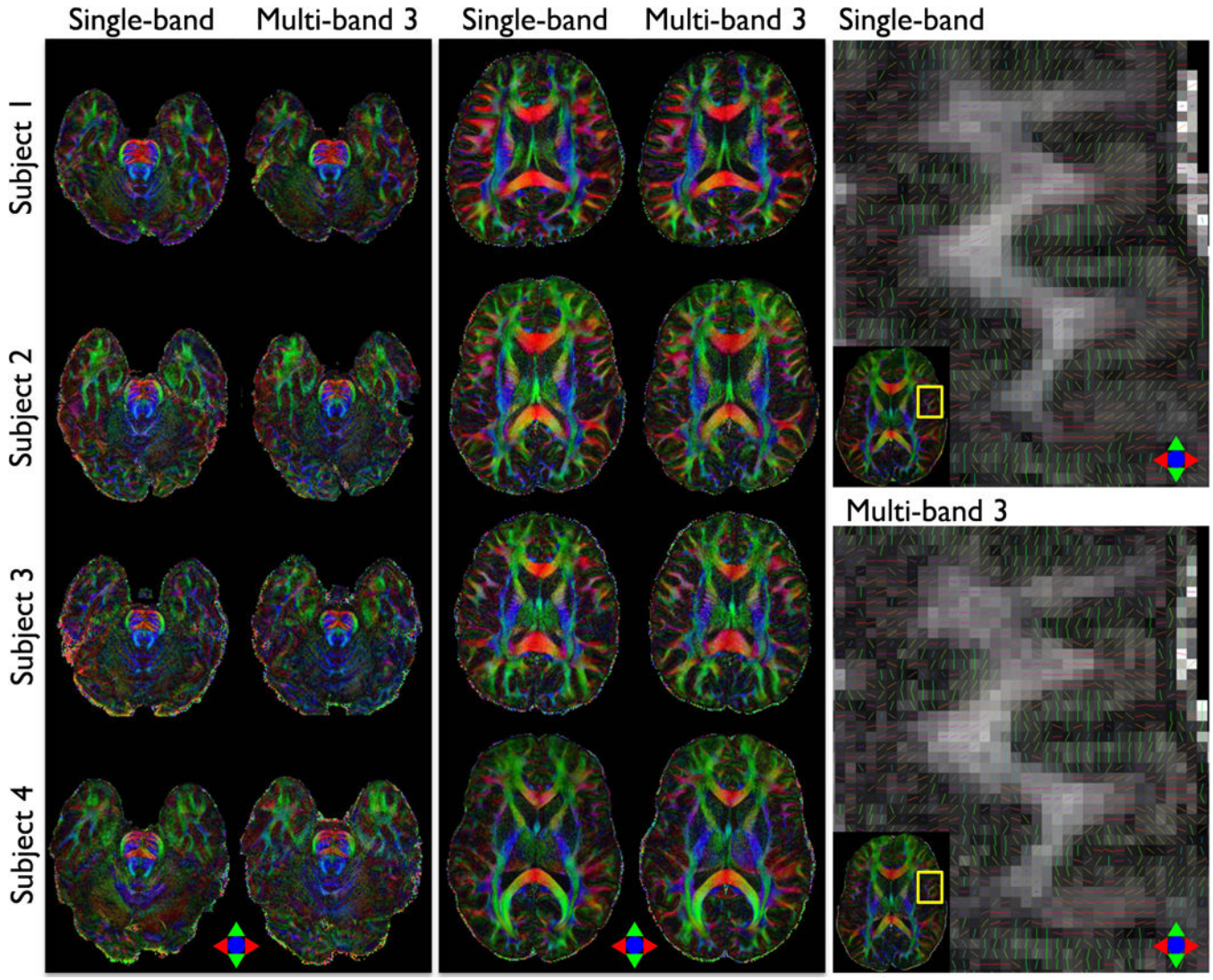

Figure 7.

Comparison of color-coded FA maps between single-band and multi-band DIADEM. Two representative slices in in-vivo brainstem (first column) and cerebrum (second column) were chosen for demonstration. A color-coded vector map was overlaid on the FA map to demonstrate the cortical diffusion anisotropy and its radial diffusion orientation in in-vivo human brain acquired with single-band and multi-band DIADEM (third column). The intrinsic (i.e., acquired) image resolution is $0.86\times0.86\times4$ mm^3 (Table 1–5 and 1–6).

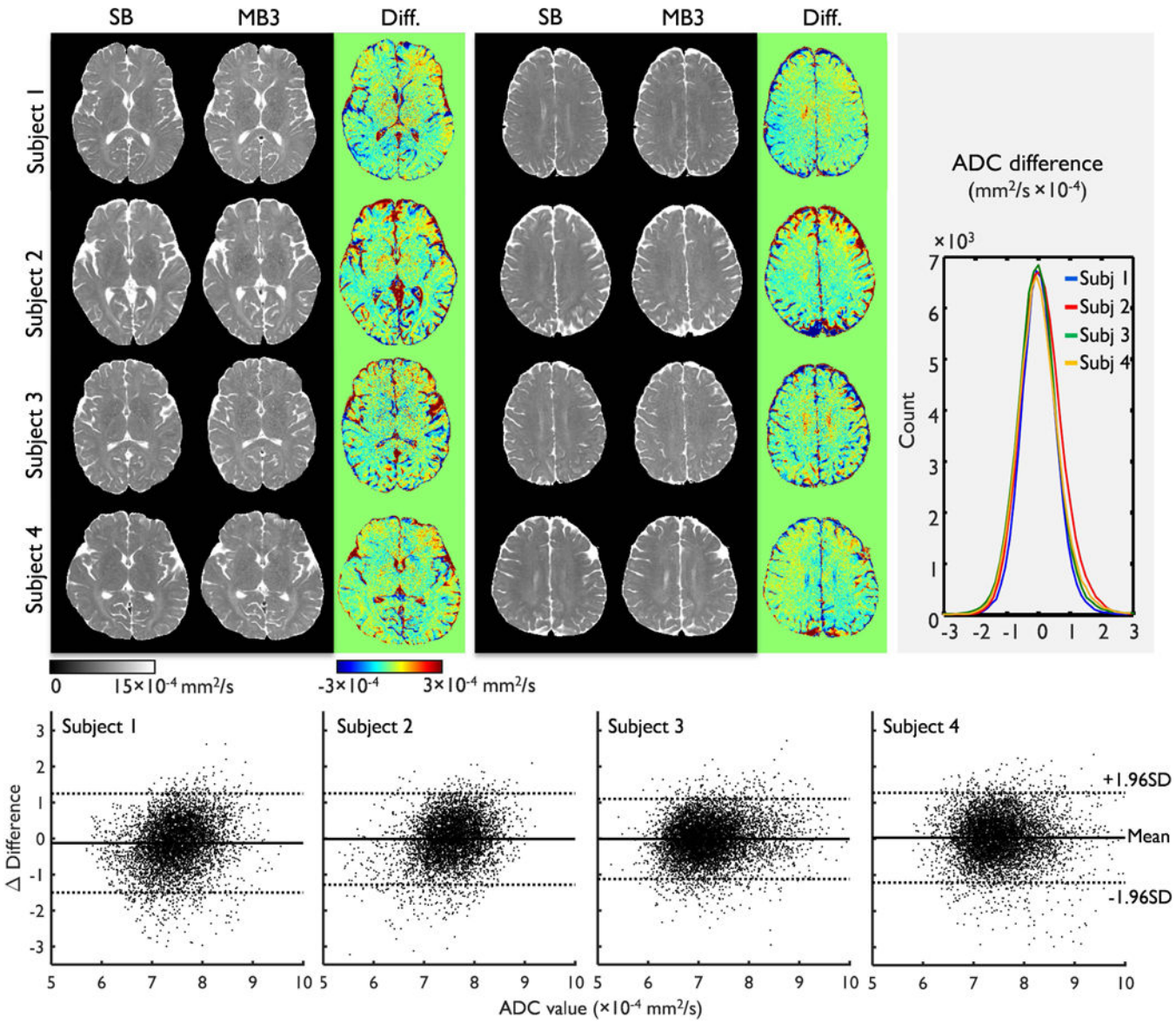

Figure 8.

Comparison of ADC maps between single-band (SB) and multi-band (MB) DIADEM. As two representative slices, central (first column, top) and superior slices (second column, top) were chosen for demonstration. Histograms (third column, top) and Bland–Altman plots (bottom row) of the ADC difference between single-band and multi-band DIADEM in white matter areas in all slices were shown. In each Bland-Altman plot, a matched and random sample of 10% (~7000 voxels) from the entire white matter area (FA>0.4 and ADC<10×10^{-4} mm^2/s) was compared for better demonstration.

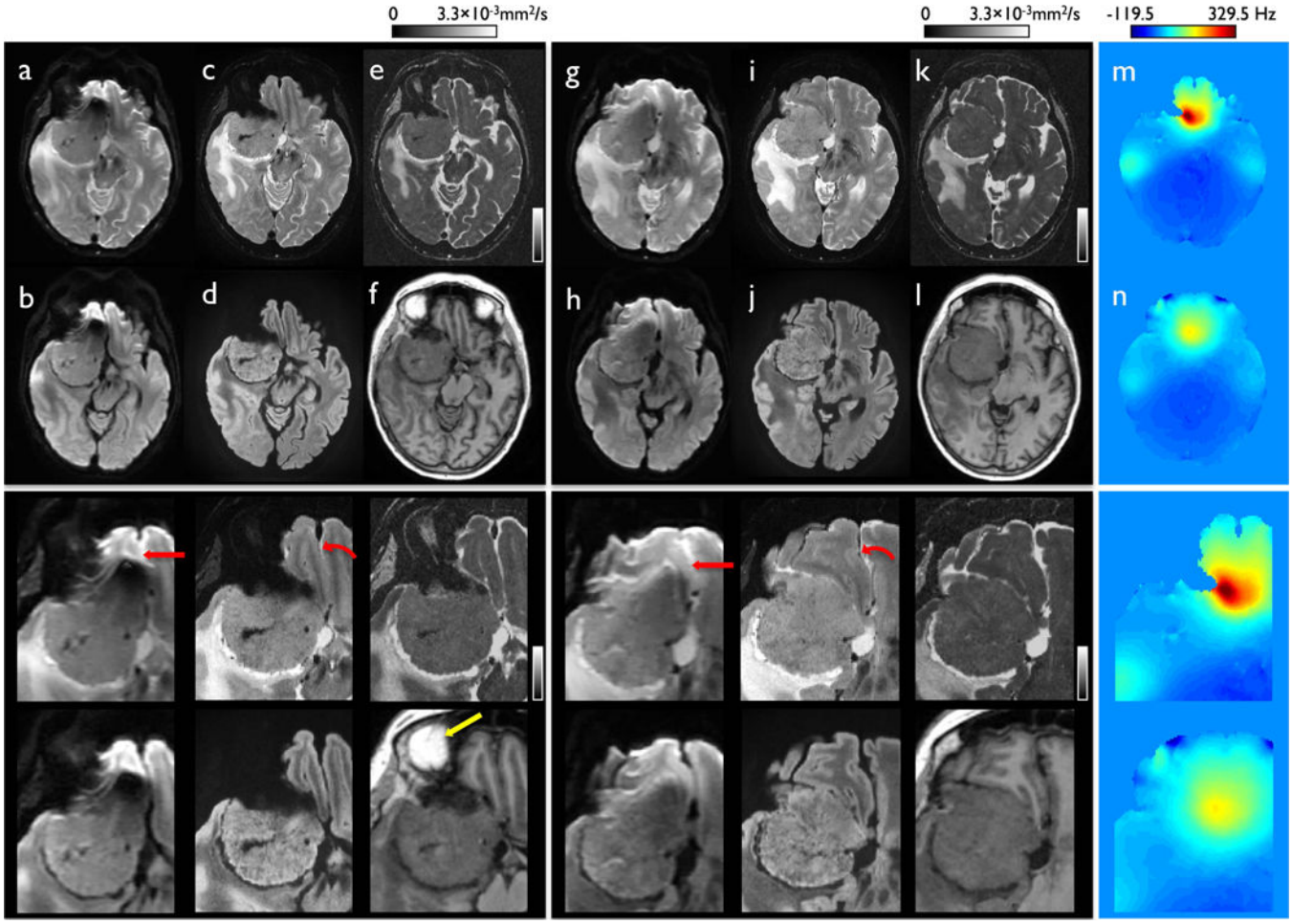

Figure 9.

DWI acquired with single-shot EPI and high spatial resolution distortion-free imaging (DIADEM) in slices with compressed (a-f) and stretched distortion (g-l) in a patient with a meningioma superior to the right orbit with the standard EPI-based non-DWI (a) and trace (b) images and DIADEM-based non-DWI (c), isoDWI (d), and MD (e) images with a corresponding image from MPRAGE (f). The off-resonance frequency maps corresponding to the slices with compressed (a-f) and stretched distortion (g-l) are shown in (m) and (n), respectively. The full FOV (upper row) and zoomed images (bottom row) are shown to demonstrate the geometrical difference between EPI (a-b and g-h) and DIADEM images (c-e and i-k) more clearly. Note that considerable distortion occurred on the EPI (arrow in a and g), which was not present when the DIADEM was used (curved arrow in c and i). Bright signal intensity seen in orbital fat surrounding the eyes is shown in the reformatted MPRAGE image (yellow arrow in f). The image resolutions for EPI, DIADEM, and MPRAGE are 1.72×0.86×4 (Table 1–8), 0.86×0.86×2.7 (Table 1–5), and 1×1.2×1 mm^3 (Table 1–11).

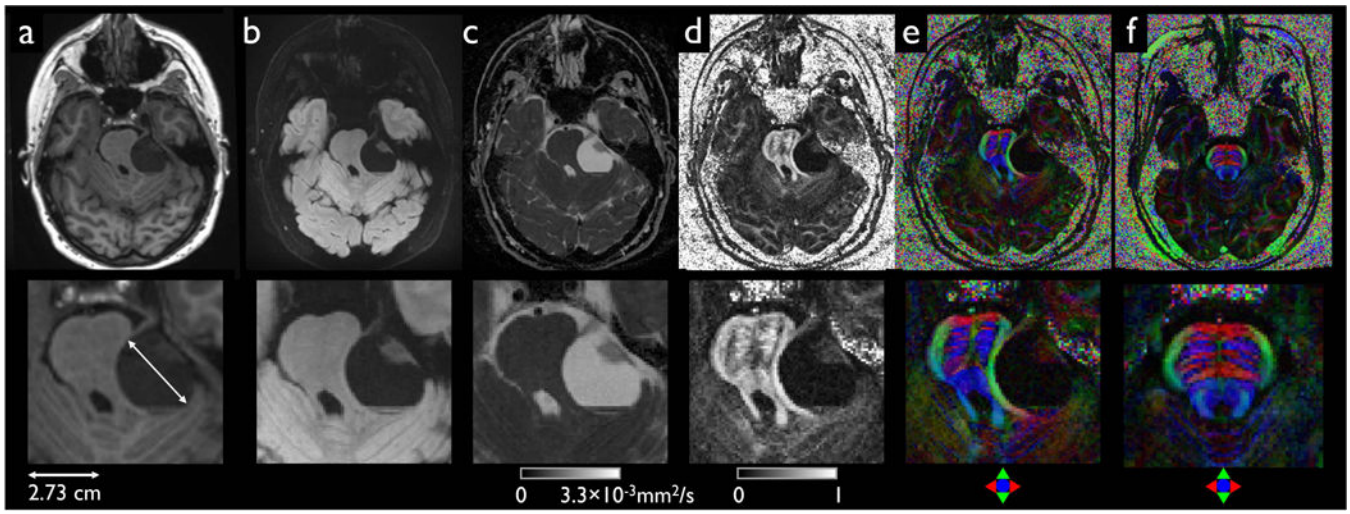

Figure 10.

Mass effect from a left vestibular schwannoma that deforms and displaces the brainstem as demonstrated with full FOV (upper row) and zoomed images (bottom row) including MPRAGE (a) and DIADEM with isoDWI (b), ADC (c), FA (d), and color-coded FA (e). A corresponding color-coded FA map obtained from a healthy volunteer is displayed in (f) for comparison. Note that identical imaging parameters in the scan for the healthy volunteer were applied, except for the reduced NE acquisition window. The acquired image resolutions for DIADEM and reformatted MPRAGE are 0.86×0.86×4 (Table 1–5) and 1×1.2×1 mm^3 (Table 1–11).

Table 1.

Experimental imaging protocols on the whole-body 3T (WB3T) and the compact 3T (C3T).

		1	2	3	4	5	6	7	8	9	10	11
Study		Comparison study			Clinical feasibility study							
Scanner		WB3T	C3T		C3T							
Sequence		2D EPI	2D EPI	2D DIADEM	2D DIADEM	2D DIADEM	2D MB-DIADEM	2D EPI	2D EPI	2D FSE	2D FLAIR	3D MPRAGE
In-plane resolution [mm^2]		0.94×0.94	0.94×0.94	0.94×0.94	1.4×1.4	0.86×0.86	0.86×0.86	0.86×0.86	1.72×0.86	0.86×0.86	0.86×0.86	1.0×1.0
Slice thickness [mm]		4.0	4.0	4.0	1.4	4.0/2.7	4.0	4.0	4.0	4.0	4.0	1.2
TI/TR/TE/*TE_{NE} [ms]		-/8850/ 72/-	-/3500/ 49.4/-	-/2388/ 47.0/56.6	-/8120/ 40.6/ 52.1	-/3096/ 42.5/57.1	-/1300/ 49.7/70.7	-/3553/ 49.1/-	-/10000/ 44.3/-	-/4450/ 86.0/-	2646.3/11000/ /148.3/-	900/6.1/ 2.5/-
Echo spacing (effective) [μs]		1056 (352)	644 (214.7)	632 (210.7)	436 (145.3)	628 (209.3)	632 (316)	628 (209.3)	436 (228)	-	-	-
FOV [mm^2]		240^2	240^2	240^2	218^2	220^2	220^2	220^2	220^2	220^2	220^2	260^2
Matrix (RO×PE)		256×256	256×256	256×256	156×156	256×256	256×256	256×256	128×256	256×256	256×256	256×256
Slices		37	37	37	109	36–38	36–38	36–38	36–38	36–38	36–38	216
Total readout BW [KHz]		250	250	250	250	250	250	250	250	31.25	31.25	31.25
Echo train length		60	60	22	26	22	48	54	80	12	24	-
Partial Fourier	EPI-PE (N_y)	0.70	0.70	1	1	1	0.75	0.63	0.63	1	1	-
Parallel imaging		3	3	3	3	3	2	3	2	2	2	2
rR (matrix size)		-	-	4 (64)	2 (78)	4 (64)	2 (128)	-	-	-	-	-
rFOV (segments)	SW-PE (N_s)	-	-	8 (32)	13 (12)	8 (32)	6 (43)	-	-	-	-	-
Partial Fourier (pF_s)		-	-	27/32	10/12	27/32	34/43	-	-	-	-	-
b-value [s/mm^2]/diffusion direction		1000/6	1000/6	1000/6	1000/6	1000/6	1000/6	1000/6	1000/3	-	-	-
Average		3	3	1	1	1	1	2	1	1	1	1
Total scan time (none/reduced NE)		3:15	1:17	7:56	9:37/8:36	9:48/8:10	5:11	0:53	0:50	1:53	6:48	4:42

*Note that TE_{NE} is the echo time for the navigator echo (NE) in the DIADEM acquisition. Two different total scan times (= TR×segments×pF_S×(diffusion directions+1) + TR (a calibration scan for EPI Nyquist ghost correction)) measured before and after the reduction in the navigator echo acquisition window are shown in the last row.